Chapter 11

Tropical Dynamics

Throughout the previous chapters of this book, we have emphasized circulation systems of the extratropical regions (i.e., the regions poleward of about 30° latitude). This emphasis should not be regarded as an indication of a lack of interesting motion systems in the tropics, but is a result, rather, of the relative complexity of the dynamics of tropical circulations. There is no simple theoretical framework analogous to quasi-geostrophic theory that can be used to provide an overall understanding of large-scale tropical motions.

Outside the tropics, the primary energy source for synoptic-scale disturbances is the zonal available potential energy associated with the latitudinal temperature gradient. Observations indicate that latent heat release and radiative heating are usually secondary contributors to the energetics of extratropical synoptic-scale systems. In the tropics, however, the storage of available potential energy is small due to the very small temperature gradients in the tropical atmosphere. Latent heat release appears to be the primary energy source, at least for those disturbances that originate within the equatorial zone. Most latent heat release in the tropics occurs in association with convective cloud systems, although much of the actual precipitation falls from mesoscale regions of stratiform clouds within such systems; the cloud systems are themselves generally embedded in large-scale circulations.

The diabatic heating associated with tropical precipitation not only drives a local response in the atmospheric circulation, but through excitation of equatorial waves may also induce a remote response. Thus, there is a strong interaction among cumulus convection, mesoscale, and large-scale circulations, which is of primary importance for understanding tropical motion systems. Furthermore, the distribution of diabatic heating in the tropics is strongly influenced by sea surface temperature (SST) variations, and these in turn are strongly influenced by the motion of the atmosphere.

An understanding of tropical circulations thus requires consideration of equatorial wave dynamics, interactions of cumulus convection and mesoscale circulations with large-scale motions, and air–sea interactions. Detailed treatment of all these topics is beyond the scope of an introductory text. Nevertheless, because the tropics play a fundamental role in the general circulation of the atmosphere, and coupling between tropical and middle latitudes is an important

An Introduction to Dynamic Meteorology. DOI: 10.1016/B978-0-12-384866-6.00011-8

consideration in extratropical extended-range forecasting, some discussion of the tropics is required even in a text with an extratropical emphasis.

Of course, it is not always possible to distinguish clearly between tropical and extratropical systems. In subtropical regions ($\sim 30^\circ$ latitude), circulation systems characteristic of both tropical and extratropical regions may be observed depending on the season and geographical location. To keep the discussion in this chapter as simple as possible, we focus primarily on the zone well equatorward of 30° latitude where the influence of middle-latitude systems should be minimum.

11.1 THE OBSERVED STRUCTURE OF LARGE-SCALE TROPICAL CIRCULATIONS

Because of the nature of their energy sources, as well as the smallness of the Coriolis parameter, large-scale equatorial motion systems have several distinctive characteristic structural features that are quite different from those of midlatitude systems. Many of these can be understood in terms of the equatorial wave modes discussed in Section 11.3. Before discussing equatorial wave theory, however, it is useful to review some of the major observed circulation features of the tropical atmosphere.

11.1.1 The Intertropical Convergence Zone

Traditionally, the tropical general circulation was thought to consist of a thermally direct Hadley circulation in which air in the lower troposphere in both hemispheres moved equatorward toward the *intertropical convergence zone* (ITCZ), where by continuity considerations it was forced to rise uniformly and move poleward, thus transporting heat away from the equator in the upper troposphere in both hemispheres. This simple model of large-scale overturning is not, however, consistent with the observed vertical profile of equivalent potential temperature (θ_e). As indicated in Figure 11.1, the mean tropical atmosphere is conditionally stable above about 600 hPa. Thus, a large-scale upward mass flow, were it to exist, would be up the gradient of θ_e in the upper troposphere and would actually *cool* the upper troposphere in the region of the ITCZ. Such a circulation could not generate potential energy and would not, therefore, satisfy the heat balance in the equatorial zone.

It appears that the only way in which heat can effectively be brought from the surface to the upper troposphere in the ITCZ is through pseudoadiabatic ascent in the cores of large cumulonimbus clouds (often referred to as "hot towers"). For such motions, cloud parcels approximately conserve θ_e. They can, therefore, arrive in the upper troposphere with moderate temperature excesses. Thus, the heat balance of the equatorial zone can be accounted for, at least qualitatively, provided that the vertical motion in the ITCZ is confined primarily to

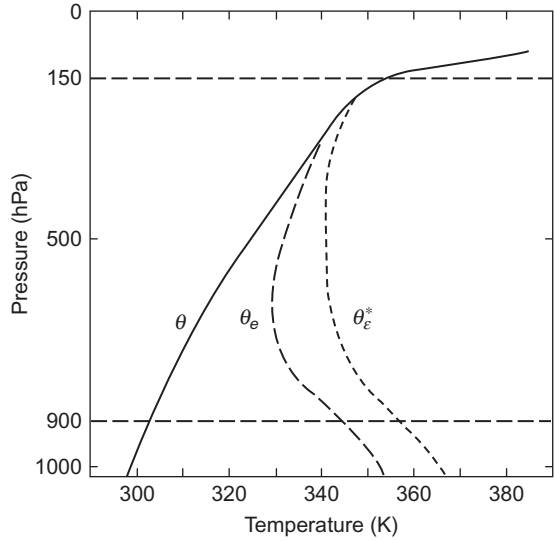

FIGURE 11.1 Typical sounding in the tropical atmosphere showing the vertical profiles of potential temperature θ, equivalent potential temperature θ_e, and equivalent potential temperature θ_ε^* of a hypothetically saturated atmosphere with the same temperature at each level. This figure should be compared with Figure 2.8, which shows similar profiles for a midlatitude squall line sounding. (*After Ooyama, 1969. Copyright © American Meteorological Society. Reprinted with permission.*)

the updrafts of individual convective cells. Riehl and Malkus (1958) estimated that only 1500–5000 individual hot towers would need to exist simultaneously around the globe to account for the required vertical heat transport in the ITCZ.

This view of the ITCZ as a narrow zonal band of vigorous cumulus convection has been confirmed beyond a doubt by observations, particularly satellite cloud photos. An example is given in Figure 11.2, which shows infrared cloud brightness temperatures in the tropics for the period August 14 to December 17, 1983. Low brightness temperatures signal the presence of deep anvil clouds characteristic of convective storms. The ITCZ appears as a line of deep convective cloud extending across the Atlantic and Pacific oceans between about 5° and 10°N.

Observations indicate that within the ITCZ, precipitation greatly exceeds the moisture supplied by evaporation from the ocean surface below. Thus, much of the vapor necessary to maintain the convection in the ITCZ must be supplied by the converging trade wind flow in the lower troposphere. In this manner the large-scale flow provides the latent heat supply required to sustain the convection. The convective heating in turn produces large-scale midtropospheric temperature perturbations and (through hydrostatic adjustment) surface and upper-level pressure perturbations, which maintain the low-level inflow.

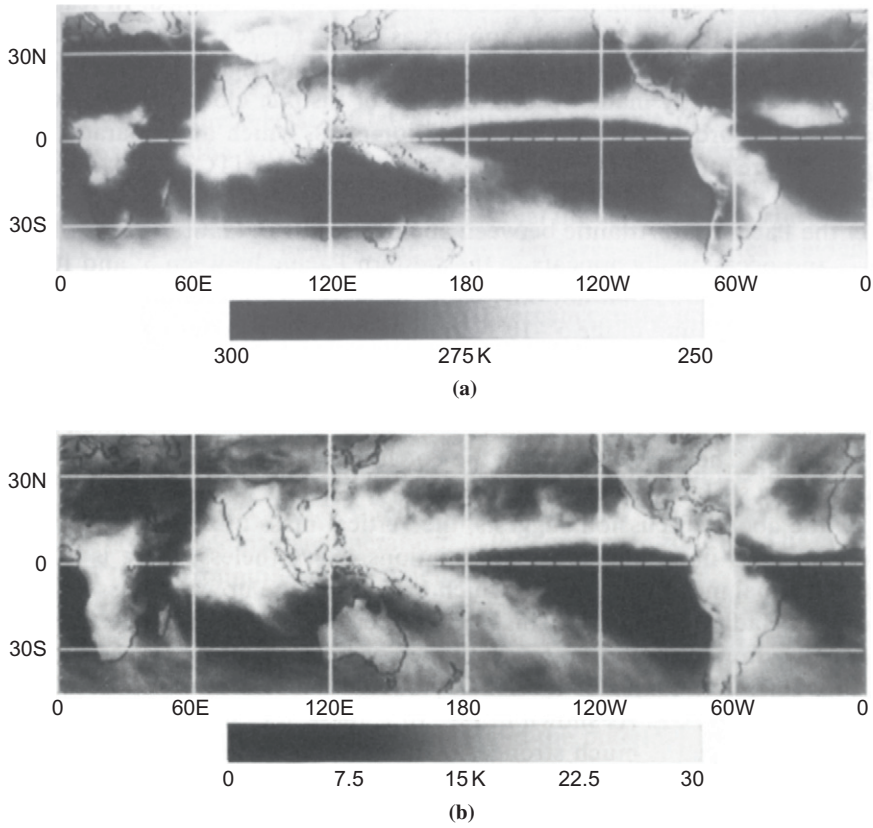

FIGURE 11.2 (a) Time-mean IR brightness temperature and (b) three-hour standard deviations about the time-mean IR brightness temperature for August 14 to December 17, 1983. Low values of brightness temperature indicate the presence of high cold cirrus anvil clouds. (*After Salby et al., 1991. Copyright © American Meteorological Society. Reprinted with permission.*)

The preceding description of the ITCZ is actually oversimplified. In reality, the ITCZ over the oceans rarely appears as a long unbroken band of heavy convective cloudiness, and it almost never is found right at the equator. Rather, it is usually made up of a number of distinct cloud clusters, with scales of the order of a few hundred kilometers, which are separated by regions of relatively clear skies. The strength of the ITCZ is also quite variable in both space and time. It is particularly persistent and well defined over the Pacific and Atlantic between about 5° and 10°N latitude (as in Figure 11.2) and occasionally appears in the western Pacific between 5° and 10°S.

Figure 11.2 shows that not only is the mean deep convection associated with the ITCZ found in the 5° to 10°N latitude belt, but during the period shown in Figure 11.2, the standard deviation of deep convection is also a maximum

there. This is consistent with the idea that the ITCZ is the locus of transient cloud clusters, rather than simply a region of steady-state precipitation and mean uplift. The dry zones along the equator in the oceanic regions are a particularly striking feature in Figure 11.2.

As the preceding discussion suggests, the vertical mass flux associated with the ITCZ has important regional variations. Nevertheless, there is a significant zonal mean component, which constitutes the upward mass flux of the mean Hadley circulation. This Hadley circulation consists of overturning thermally direct cells in the low latitudes of both hemispheres, as shown in Figure 10.7. The center of the Hadley circulation is located at the mean latitude of the ITCZ. As Figure 10.7 shows, the winter hemisphere branch of the Hadley cell is much stronger than the summer hemisphere branch. Observations indicate that two Hadley cells, symmetric about the equator, are rarely observed even in the equinoctial seasons. Rather, the northern cell dominates from November to March, the southern cell dominates from May to September, and rapid transitions occur in April and October (see Oort, 1983).

11.1.2 Equatorial Wave Disturbances

The variance observed in the cloudiness associated with the ITCZ, as illustrated in Figure 11.2b, is generally caused by transient precipitation zones associated with weak equatorial wave disturbances that propagate westward along the ITCZ. That such westward-propagating disturbances exist and are responsible for a large part of the cloudiness in the ITCZ can be seen easily by viewing time-longitude sections constructed from daily satellite pictures cut into thin zonal strips. An example is shown in Figure 11.3. The well-defined bands of cloudiness that slope from right to left down the page define the locations of the cloud clusters as functions of longitude and time. Clearly much of the cloudiness in the 5 to 10°N latitude zone of the Pacific is associated with westward-moving disturbances. The slope of the cloud lines in Figure 11.3 implies a westward propagation speed of about 8 to 10 $\mathrm{m\,s^{-1}}$. The longitudinal separation of the cloud bands is about 3000 to 4000 km, corresponding to a period range of about 4 to 5 days for this type of disturbance.

Diagnostic studies suggest that these westward-propagating wave disturbances are generally driven by the release of latent heat in their accompanying convective precipitation areas. The vertical structure of a typical equatorial wave disturbance is shown in schematic form in Figure 11.4. Vertical motion in such disturbances is proportional to the diabatic heating rate; thus, the maximum vertical velocities occur in the convective zone. By mass continuity there must be convergence at low levels in the convective zone and divergence in the upper levels. Hence, provided that the absolute vorticity has the sign of f, the divergence term in the vorticity equation will induce cyclonic vorticity tendencies in the lower troposphere and anticyclonic vorticity tendencies in the upper

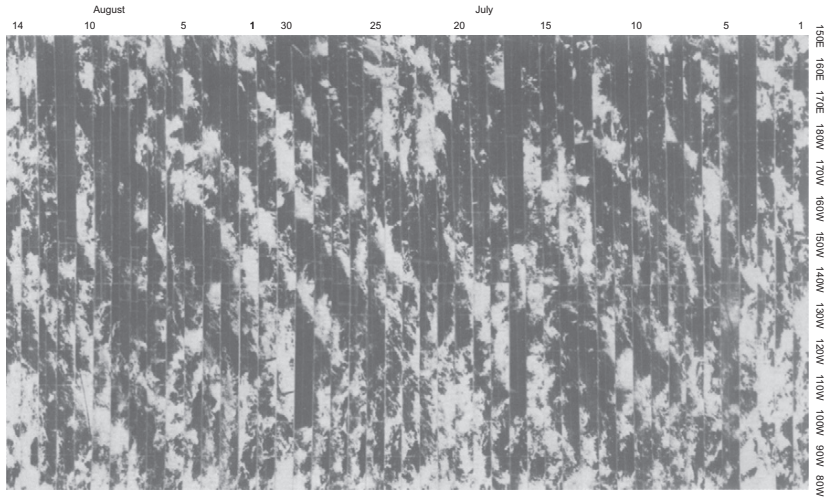

FIGURE 11.3 Time-longitude sections of satellite photographs for the period July 1 to August 14, 1967, in the 5 to 10°N latitude band of the Pacific. The westward progression of the cloud clusters is indicated by the bands of cloudiness sloping down the page from right to left. (*After Chang, 1970. Copyright © American Meteorological Society. Reprinted with permission.*)

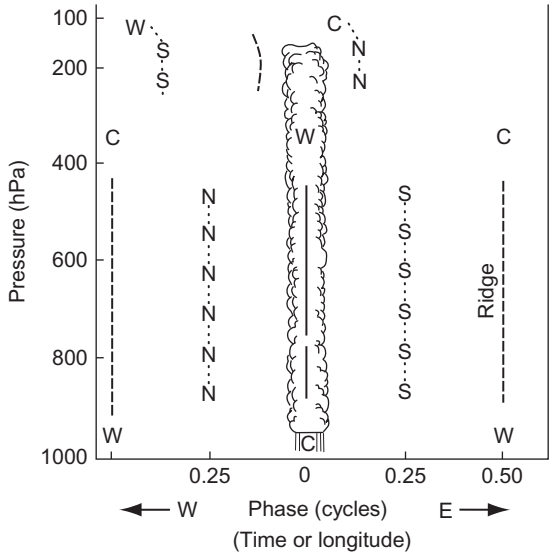

FIGURE 11.4 Schematic model for equatorial wave disturbances showing trough axis (*solid line*), ridge axis (*dashed lines*), and axes of northerly and southerly wind components (*dotted lines*). Regions of warm and cold air are designated by W and C, respectively. The axes shown are for northerly (N) and southerly (S) wind components. (*After Wallace, 1971. Copyright © American Geophysical Union. Used with permission.*)

troposphere. The process of adjustment between mass and velocity fields will then generate a low-level trough and an upper-level ridge.[1] Thus, the thickness (or layer mean temperature) in the convective zone must be greater than in the surrounding environment.

In the convectively active areas of equatorial waves there is net upward motion, and midtropospheric temperatures are warmer than average (although generally by less than 1°C). The correlations between temperature and vertical motion, and between temperature and diabatic heating, are thus both positive, and the potential energy generated by the diabatic heating is immediately converted to kinetic energy—that is, the $P' \cdot K'$ conversion balances R' in (10.62). There is, in this approximation, no storage in the form of available potential energy. The energy cycle of these disturbances, therefore, differs remarkably from that of midlatitude baroclinic systems in which the available potential energy greatly exceeds the kinetic energy.

For latent heat release by cumulonimbus clouds to be an effective energy source for large-scale disturbances, there must be an interaction between the convective scale and the large scale, as mentioned in Section 9.7.2. In such interaction large-scale convergence at low levels moistens and destabilizes the environment so that small-scale thermals can easily reach the level of free convection and produce deep cumulus convection. The cumulus cells, in turn, act cooperatively to provide the large-scale heat source that drives the secondary circulation responsible for the low-level convergence.

A typical vertical profile of divergence in the precipitation zone of a synoptic-scale equatorial wave disturbance in the western Pacific is shown in Figure 11.5. Convergence is not limited to low-level frictional inflow in the planetary boundary layer, but extends up to nearly 400 hPa, which is the height where the hot towers achieve their maximum buoyancy. The deep convergence implies that there must be substantial entrainment of midtropospheric air into the convective cells. Because the midtropospheric air is relatively dry, this entrainment will require considerable evaporation of liquid water to bring the mixture of cloud and environment air to saturation. It will thus reduce the buoyancy of the cloud air and may in fact produce negatively buoyant convective downdrafts if there is sufficient evaporative cooling. However, in the large cumulonimbus clouds present in equatorial waves, the central core updrafts are protected from entrainment by the surrounding cloud air so that they can penetrate nearly to the tropopause without dilution by environmental air. These undiluted cores constitute the "hot towers" referred to in Section 11.1.1. Because the hot towers are responsible for much of the vertical heat and mass transport above the boundary

[1] The terms *trough* and *ridge* as used by tropical meteorologists designate pressure minima and maxima, respectively, just as in midlatitudes. In the easterlies of the Northern Hemisphere tropics, however, the zonal-mean pressure increases with latitude so that the pattern of isobars depicting a tropical trough will resemble the pattern associated with a ridge in middle latitudes (i.e., there is a poleward deflection of the isobars).

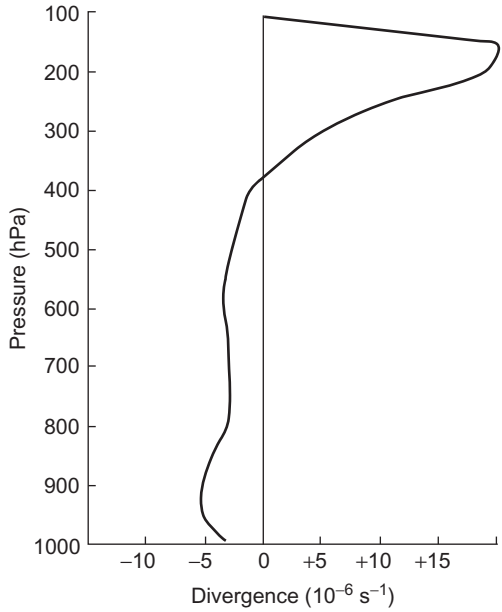

FIGURE 11.5 Vertical profile of 4°-square area average divergence based on composites of many equatorial disturbances. (*Adapted with permission from Williams, 1971.*)

layer in the ITCZ, and the wave disturbances contain most of the active convective precipitation areas along the ITCZ, it is obvious that equatorial waves play an essential role in the general circulation of the atmosphere.

11.1.3 African Wave Disturbances

The considerations of the previous subsection are valid for ITCZ disturbances over most regions of the tropical oceans. In the region of the North African continent, however, local effects due to surface conditions create a unique situation that requires separate discussion. During the Northern Hemisphere summer, intense surface heating over the Sahara generates a strong positive meridional temperature gradient in the lower troposphere between the equator and about 25°N. The resulting easterly thermal wind is responsible for the existence of a strong easterly jet core near 650 hPa centered near 16°N as shown in Figure 11.6. Synoptic-scale disturbances are observed to form and propagate westward in the cyclonic shear zone to the south of this jet core.

Occasionally, such disturbances are progenitors of tropical storms and hurricanes in the western Atlantic. The average wavelength of observed African wave disturbances is about 2500 km, and the westward propagation speed is about 8 ms^{-1}, implying a period of about 3.5 days. The disturbances have horizontal velocity perturbations that reach maximum amplitude at the 650-hPa

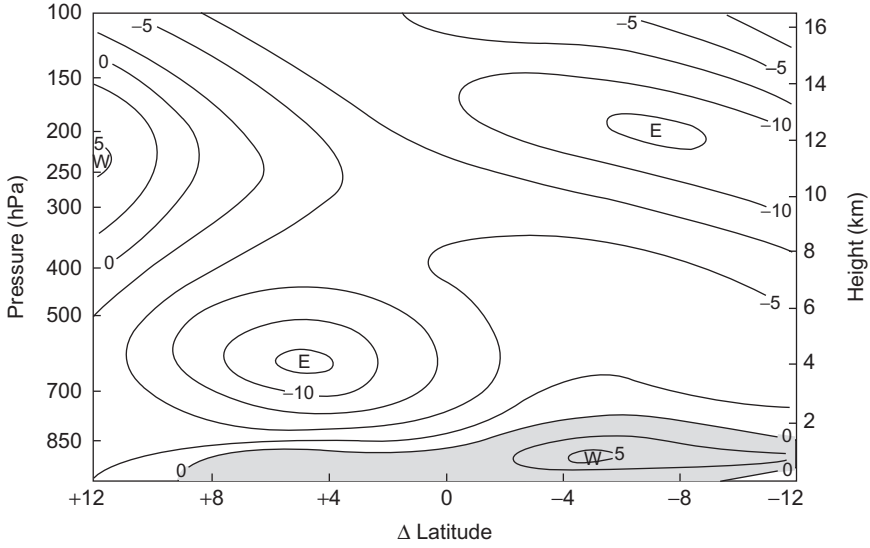

FIGURE 11.6 Mean-zonal wind distribution in the North African region (30°W to 10°E longitude) for the period August 23 to September 19, 1974. Latitude is shown relative to latitude of maximum disturbance amplitude at 700 hPa (about 12°N). The contour interval is 2.5 m s^{-1}. (*After Reed et al., 1977. Copyright © American Meteorological Society. Reprinted with permission.*)

level, as indicated in Figure 11.7. Although there is considerable organized convection associated with these waves, they do not appear to be driven primarily by latent heat release, but depend, rather, on barotropic and baroclinic conversions of energy from the easterly jet.

In Figure 11.8 the absolute vorticity profile for the African easterly jet shown in Figure 11.6 is plotted. The shaded region indicates the area in which the vorticity gradient is negative. Thus, it is clear that the African jet satisfies the necessary condition for barotropic instability discussed in Section 7.4.2.[2] Baroclinic instability due to the strong easterly shear in the lower troposphere also appears to play a role in these disturbances. Thus, both barotropic and baroclinic conversions from the mean flow energy appear to be important for the generation of African wave disturbances.

Because such disturbances continue to exist in the absence of strong mean wind shears after they have propagated westward into the Atlantic, it is unlikely that either baroclinic or barotropic instability continues to be the primary energy source for their maintenance. Rather, diabatic heating through precipitating

[2]It should be noted here that the profile shown in Figure 11.6 is not a zonal mean. Rather, it is a time mean for a limited longitudinal domain. Provided that the longitudinal scale of variation of this time-mean zonal flow is large compared to the scale of the disturbance, the time-mean flow may be regarded as a locally valid basic state for linear stability calculations.

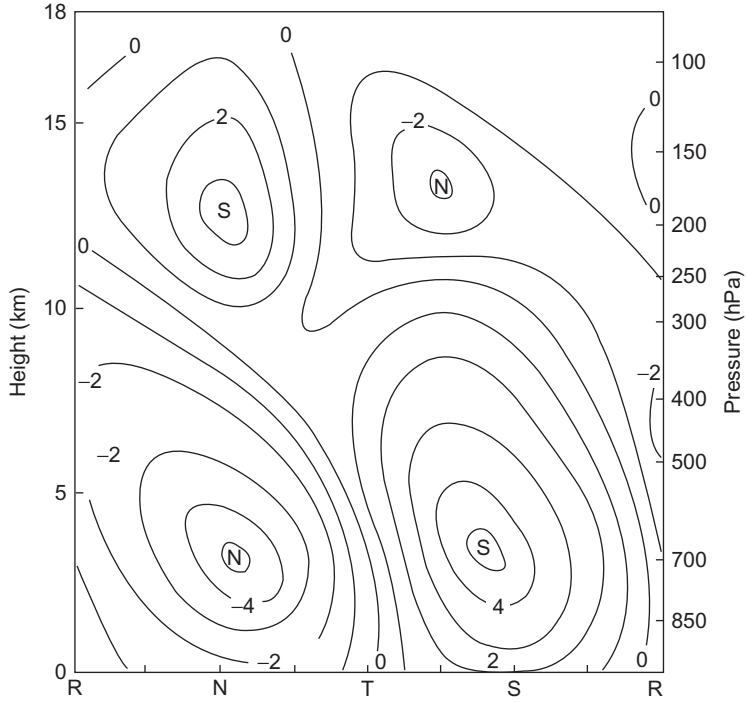

FIGURE 11.7 Vertical cross-section along the reference latitude of Figure 11.6 showing perturbation meridional velocities in $m\,s^{-1}$. R, N, T, and S refer to ridge, northwind, trough, and southwind sectors of the wave, respectively. (*After Reed et al., 1977. Copyright © American Meteorological Society. Reprinted with permission.*)

convective systems appears to be the main energy source for such waves over the ocean.

11.1.4 Tropical Monsoons

The term *monsoon* is commonly used in a rather general sense to designate any seasonally reversing circulation system. The basic drive for a monsoon circulation is provided by the contrast in the thermal properties of the land and sea surfaces. Because the thin layer of soil that responds to seasonal changes in surface temperature has a small heat capacity compared to the heat capacity of the upper layer of the ocean that responds on a similar timescale, the absorption of solar radiation raises the surface temperature over land much more rapidly than over the ocean. The warming of the land relative to the ocean leads to enhanced cumulus convection and thus to latent heat release, which produces warm temperatures throughout the troposphere.

Much of the tropics is influenced by monsoons. The most extensive monsoon circulation by far is the Asian monsoon. This monsoon completely dominates

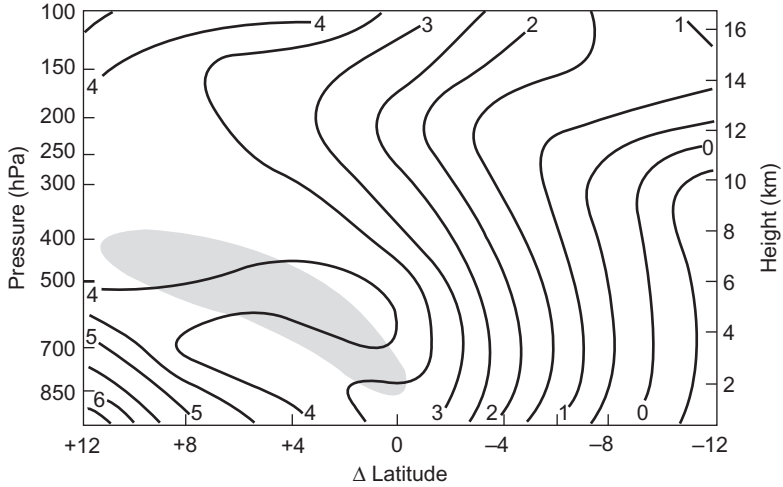

FIGURE 11.8 Absolute vorticity (units $10^{-5}s^{-1}$) corresponding to the mean wind field of Figure 11.6. Shading shows region where $\beta - \partial^2\bar{u}/\partial y^2$ is negative. (*After Reed et al., 1977. Copyright © American Meteorological Society. Reprinted with permission.*)

the climate of the Indian subcontinent, producing warm wet summers and cool dry winters. An idealized model of the structure of the Asian summer monsoon is indicated in Figure 11.9. As indicated in Figure 11.9, the 1000 to 200-hPa thickness is larger over the land than over the ocean. As a result there is a pressure gradient force at the upper levels directed from the land to the ocean.

The divergent wind that develops in response to this pressure gradient (shown by the arrows in Figure 11.9) causes a net mass transport out of the air column above the continent and thereby generates a surface low over the continent (often called a *thermal low*). A compensating convergent wind then develops at low levels. This low-level flow produces a convergence of moisture, which by increasing the equivalent potential temperature in the boundary layer makes the environment more favorable for development of the cumulus convection, which is the primary energy source for the monsoon circulation.

The low-level convergence and upper-level divergence over the continent constitute a secondary circulation that concentrates cyclonic vorticity at the lower levels and anticyclonic vorticity at the upper levels. Thus, the vorticity adjusts toward geostrophic balance. From Figure 11.9 it is clear that a positive correlation exists between the vertical motion and the temperature field. Therefore, the monsoon circulation converts eddy potential energy to eddy kinetic energy, just as midlatitude baroclinic eddies do.

Unlike the case of baroclinic eddies, however, the primary energy cycle of the monsoons does not involve the zonal-mean potential or kinetic energy. Rather, eddy potential energy is generated directly by diabatic heating (latent and radiative heating); the eddy potential energy is converted to eddy kinetic

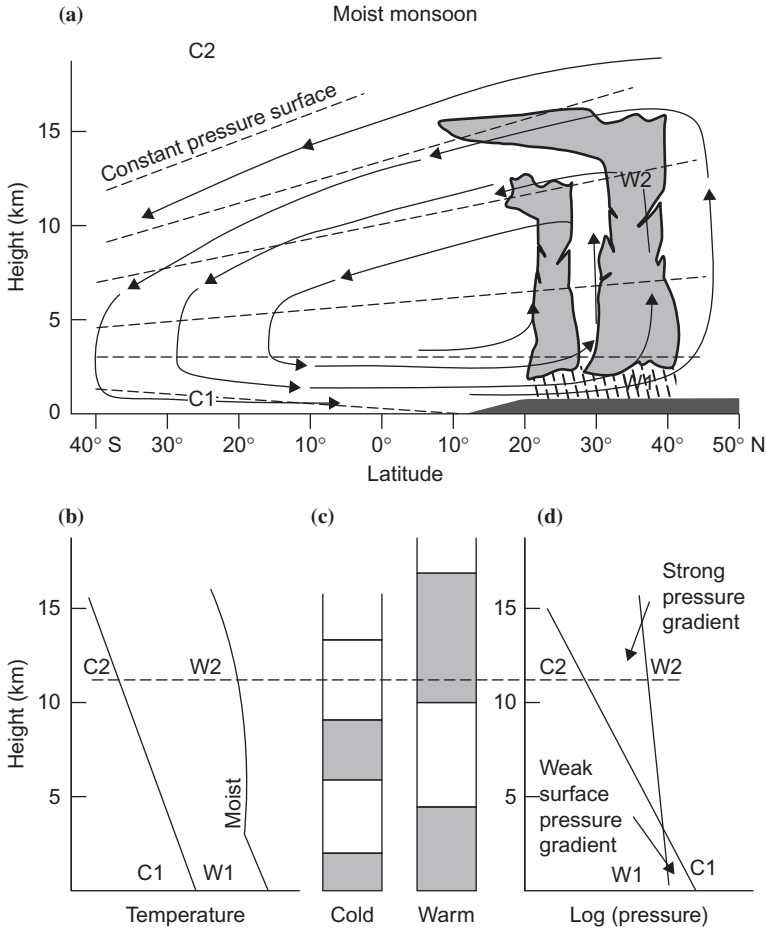

FIGURE 11.9 Schematic representation of the moist phase of the Asian monsoon. (a) *Arrows* show the meridional circulation, *dashed lines* the isobars. (b) Temperature profiles for columns C1 to C2 and W1 to W2, respectively. (c) Schematic of the mass distribution in the cold and warm sectors. (d) Horizontal pressure difference as a function of height. (*After Webster and Fasullo, 2003.*)

energy by a thermally direct secondary circulation; and the eddy kinetic energy is frictionally dissipated. (A portion of the eddy kinetic energy may be converted to zonal kinetic energy.) In a dry atmosphere, monsoon circulations would still exist; however, because the diabatic heating would then be confined to a shallow layer near the surface, they would be much weaker than the observed monsoons. The presence of cumulus convection and its concomitant latent heat release greatly amplifies the eddy potential energy generation and makes the summer monsoons among the most important features of the global circulation.

In the winter season the thermal contrast between the land and the sea reverses so that the circulation is just opposite to that shown in Figure 11.9. As a result the continents are cool and dry and the precipitation is found over the relatively warm oceans.

11.1.5 The Walker Circulation

The pattern of diabatic heating in the equatorial regions exhibits strong departures from zonal symmetry. These are caused by longitudinal variations in sea surface temperature due mainly to the effects of wind-driven ocean currents. Such SST variations produce zonally asymmetric atmospheric circulations, which in some regions dominate over the Hadley circulation. Of particular significance is the east–west overturning along the equator, which is shown schematically in Figure 11.10. Several overturning cells are indicated, which are associated with diabatic heating over equatorial Africa, Central and South America, and the Maritime Continent (i.e., the Indonesian region). The dominant cell in both zonal scale and amplitude, however, is that in the equatorial Pacific. This cell is referred to as *Walker circulation* after G. T. Walker, who first documented the surface pressure pattern associated with it.

As suggested by Figure 11.10, this pressure pattern consists of low surface pressure in the western Pacific and high surface pressure in the eastern Pacific.

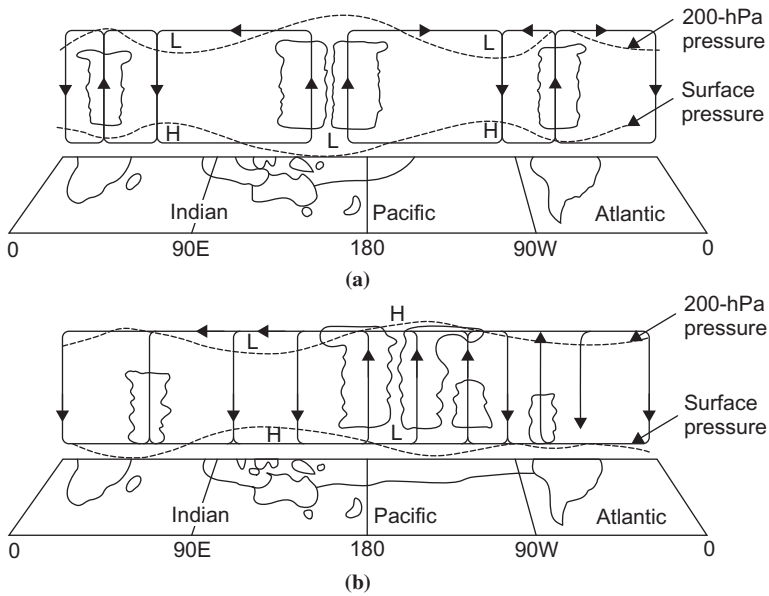

FIGURE 11.10 Schematic diagrams of the Walker circulations along the equator for (a) normal conditions and (b) El Niño conditions. (*From Webster, 1983, and Webster and Chang, 1988. Copyright © American Meteorological Society. Reprinted with permission.*)

The resulting westward-directed pressure gradient force drives mean surface easterlies in the equatorial Pacific, which are much stronger than the zonal-mean surface easterlies, and by horizontal vapor transport provides a moisture source for convection in the western Pacific, in addition to that provided by the high evaporation rates caused by the high sea surface temperatures in that region.

The wind stress due to the time-mean equatorial easterly surface winds over the Pacific has a strong influence on the heat balance of the ocean surface layer. It advects warm surface waters into the western Pacific and produces poleward drifts in the oceanic Ekman layer which by continuity drive an equatorial upwelling. This upwelling accounts for the cold tongue of water along the equator, which in turn is a major reason for the equatorial dry zone exhibited earlier in Figure 11.2.

11.1.6 El Niño and the Southern Oscillation

The east–west pressure gradient associated with the Walker circulation undergoes an irregular interannual variation. This global-scale "see-saw" in pressure, and its associated changes in patterns of wind, temperature, and precipitation, was named the *southern oscillation* by Walker. This oscillation can be clearly seen by comparing time series of surface pressure anomalies (i.e., departures from the long-term mean) for locations on the western and eastern sides of the equatorial Pacific. As shown in the upper portion of Figure 11.11, surface pressure anomalies at Darwin, Australia, and Tahiti are negatively correlated and have strong variations in the period range of 2 to 5 years. During periods of large pressure difference between these stations, the Walker circulation is unusually strong and has the same general structure as its time-mean pattern. In periods of weak pressure difference the Walker circulation weakens and the region of maximum rainfall shifts eastward (see Figure 11.10b).

The weakening of trade winds during periods of small Darwin–Tahiti pressure difference reduces wind-driven oceanic upwelling and deepens the oceanic thermocline in the eastern Pacific. This in turn, as shown in the lower portion of Figure 11.11, leads to an increase in the sea surface temperature that is referred to as *El Niño* (Spanish for "the child"). This term was originally applied to a warming of the coastal waters of Peru and Ecuador that occurs annually near Christmas time (hence, El Niño refers to the Christ child), but is now used in a more general sense for the large-scale oceanic anomalies associated with the weak wind phase of the Southern Oscillation. In the opposite phase, the strengthening of trade winds associated with large Darwin–Tahiti pressure differences enhances oceanic upwelling and deepens the oceanic thermocline. This causes a cooling of the sea surface temperatures in the equatorial Pacific that is now referred to as *La Niña*.

The ocean anomalies associated with weakening in the trade winds may begin near the coast, but over the course of several months spread westward along the equator to produce large-scale positive SST anomalies over much of

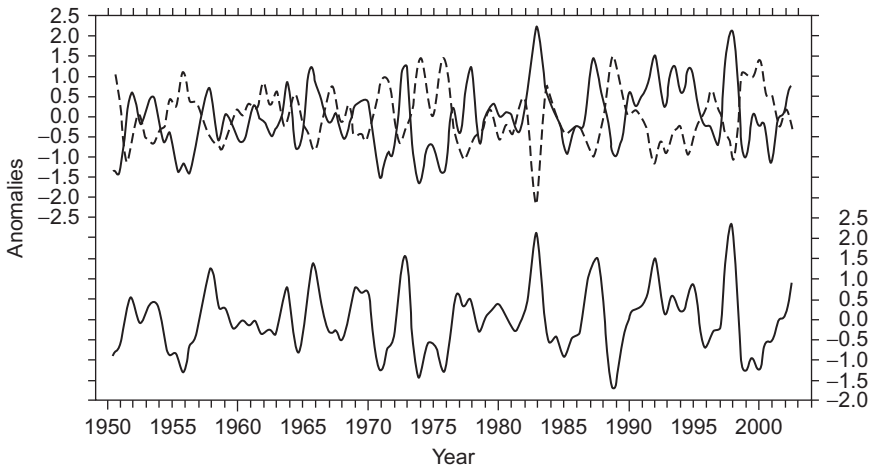

FIGURE 11.11 Time series showing SST anomalies (°C) in the eastern Pacific (*lower curve*) and anomalies in sea-level pressures (hPa) at Darwin (*upper solid curve*) and Tahiti (*upper dashed curve*). Data are smoothed to eliminate fluctuations with periods less than a year. (*Figure courtesy of Dr. Todd Mitchell, University of Washington.*)

the equatorial Pacific. These SST anomalies in turn cause a further weakening of the trade winds. This entire complex of atmospheric and oceanic variations is now referred to as ENSO (for El Niño—Southern Oscillation). It is a dramatic example of interannual climate variability associated with atmosphere–ocean coupling.

The leading theoretical model for ENSO is the "delayed oscillator" model. In this model the sea surface temperature anomaly, T, in the eastern Pacific satisfies an equation of the form

$$\frac{dT}{dt} = bT(t) - cT(t - \tau)$$

where b and c are positive constants and τ is a time delay determined by the adjustment time for the equatorial ocean. The first term on the right represents a positive feedback associated with changes in the Darwin–Tahiti pressure difference. This term represents the atmosphere–ocean coupling through which an initial weakening of the wind causes an increase of the SST, which induces a further weakening of the wind and thus a further increase in the SST. The second term provides a negative feedback due to the adjustment in the thermocline depth (and thus the ocean temperature) caused by propagating equatorial waves (see Section 11.4) in the ocean that are excited by the SST changes. The time delay in the negative feedback term is determined by the time that it takes for wave energy excited by air–sea interaction in the eastern Pacific to propagate to the western boundary of the ocean, undergo reflection, and propagate back to the region of origin. For realistic parameters the delayed oscillator model leads

to ENSO oscillations in the period range of 3 to 4 years. This highly simplified model qualitatively accounts for the average characteristics of an ENSO cycle, but cannot, however, account for the observed irregularity of ENSO.

In addition to its profound effects in the equatorial region, ENSO is associated with a wide range of interannual climate anomalies in the extratropics. Thus, the development of models that show skill in predicting ENSO several months in advance is of considerable practical importance.

11.1.7 Equatorial Intraseasonal Oscillation

In addition to the interannual variability associated with El Niño, the equatorial circulation has an important intraseasonal oscillation, which occurs on a timescale of 30 to 60 days and is often referred to as the Madden–Julian oscillation (MJO) in honor of the meteorologists who first described it. The structure of the equatorial intraseasonal oscillation is shown schematically in Figure 11.12, which shows the time development of the oscillation in the form of longitude–height sections along the equator, with time increasing at an interval of about 10 days for each panel from top to bottom. The circulations in Figure 11.12 are intended to represent anomalies from the time-mean equatorial circulation.

The oscillation originates with the development of a surface low-pressure anomaly over the Indian Ocean, accompanied by enhanced boundary layer moisture convergence, increased convection, warming of the troposphere, and raising of the tropopause height. The anomaly pattern gradually moves eastward at about 5 m s^{-1} and reaches maximum intensity over the western Pacific. As the anomaly moves over the cooler waters of the central Pacific, the anomalous convection gradually weakens, although a circulation disturbance continues eastward and can sometimes be traced completely around the globe. The observed intraseasonal oscillation is known to be associated with equatorial Rossby and Kelvin waves (see Section 11.4). However, a completely satisfactory theory for the oscillation has not yet been developed.

11.2 SCALE ANALYSIS OF LARGE-SCALE TROPICAL MOTIONS

Despite the uncertainties involved in the interaction between convective and synoptic scales, some information on the character of synoptic-scale motions in the tropics can be obtained through the methods of scale analysis. The scaling arguments can be carried out most conveniently if the governing equations are written in the log-pressure coordinate system introduced in Section 7.4.1:

$$\left(\frac{\partial}{\partial t} + \mathbf{V}\cdot\nabla + w^*\frac{\partial}{\partial z^*}\right)\mathbf{V} + f\mathbf{k}\times\mathbf{V} = -\nabla\Phi \tag{11.1}$$

$$\partial\Phi/\partial z^* = RT/H \tag{11.2}$$

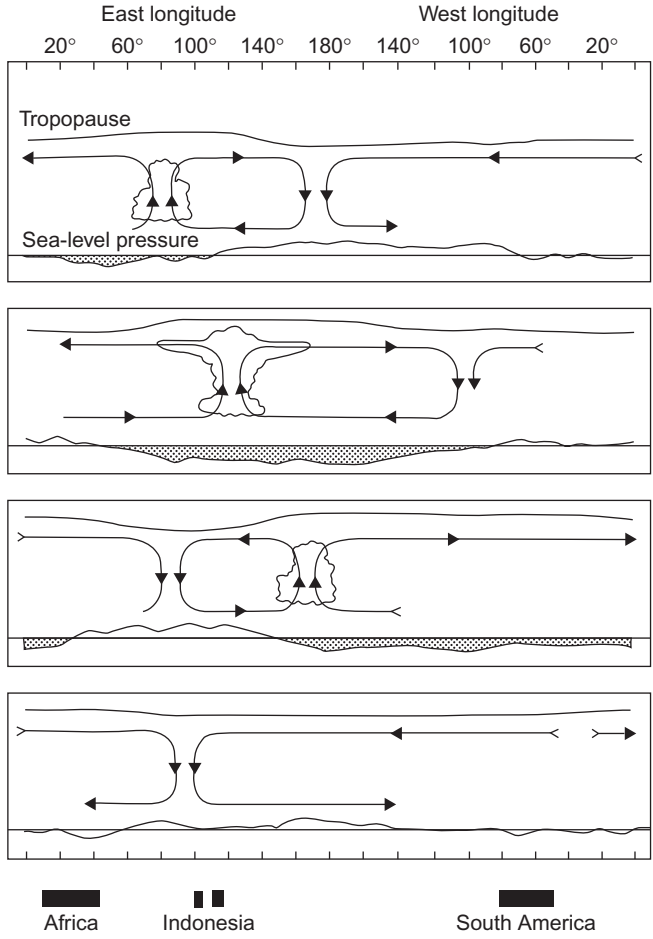

FIGURE 11.12 Longitude-height section of the anomaly pattern associated with the tropical intraseasonal oscillation (MJO). Reading downward, the panels represent a time sequence with intervals of about 10 days. *Streamlines* show the west–east circulation, the *wavy top line* represents the tropopause height, and the *bottom line* represents surface pressure (with *shading* showing below-normal surface pressure). (*After Madden, 2003; adapted from Madden and Julian, 1972.*)

$$\partial u/\partial x + \partial v/\partial y + \partial w^*/\partial z^* - w^*/H = 0 \tag{11.3}$$

$$\left(\frac{\partial}{\partial t} + \mathbf{V}\cdot\nabla\right) T + w^* N^2 H/R = J/c_p \tag{11.4}$$

We wish to compare the magnitudes of the various terms in (11.1) through (11.4) for synoptic-scale motions in the tropics. We first note that an upper limit on the vertical velocity scale W is imposed by the continuity equation (11.3).

Thus, following the discussion of Section 4.5,

$$\partial u/\partial x + \partial v/\partial y \leq U/L$$

However, for motions with vertical scales comparable to the density scale height H,

$$\partial w^*/\partial z^* - w^*/H \sim W/H$$

so that the vertical velocity scale must satisfy the constraint $W \leq HU/L$ if the horizontal divergence and the vertical stretching terms are to balance in the continuity equation. We next define characteristic scales for the various field variables as follows:

$H \sim 10^4$ m	vertical length scale
$L \sim 10^6$ m	horizontal length scale
$U \sim 10\,\mathrm{m\,s^{-1}}$	horizontal velocity scale
$W \leq HU/L$	vertical velocity scale
$\delta\Phi$	geopotential fluctuation scale
$L/U \sim 10^5$ s	timescale for advection

The magnitudes chosen for the horizontal length and velocity scales are typical for observed values in synoptic-scale systems both in the tropics and at midlatitudes. We now wish to show how the corresponding characteristic scales for vertical velocity and geopotential fluctuations are limited by the dynamic constraints imposed by conservation of mass, momentum, and thermodynamic energy.

We can estimate the magnitude of the geopotential fluctuation $\delta\Phi$ by scaling the terms in the momentum equation (11.1). For this purpose it is convenient to compare the magnitude of the horizontal inertial acceleration,

$$(\mathbf{V}\cdot\nabla)\mathbf{V} \sim U^2/L$$

with each of the other terms in (11.1) as follows:

$$|\partial\mathbf{V}/\partial t| \,/\, |(\mathbf{V}\cdot\nabla)\mathbf{V}| \sim 1 \tag{11.5}$$

$$|w^*\partial\mathbf{V}/\partial z^*| / |(\mathbf{V}\cdot\nabla)\mathbf{V}| \sim WL/UH \leq 1 \tag{11.6}$$

$$|f\mathbf{k}\times\mathbf{V}| \,/\, |(\mathbf{V}\cdot\nabla)\mathbf{V}| \sim fL/U = \mathrm{Ro}^{-1} \leq 1 \tag{11.7}$$

$$|\nabla\Phi| \,/\, |(\mathbf{V}\cdot\nabla)\mathbf{V}| \sim \delta\Phi/U^2 \tag{11.8}$$

We have shown previously that in middle latitudes where $f \sim 10^{-4}\,\mathrm{s}^{-1}$, the Rossby number Ro is small so that to first approximation the Coriolis force and pressure gradient force terms balance. In that case, $\delta\,\Phi \sim fUL$. In the equatorial region, however, $f \leq 10^{-5}\,\mathrm{s}^{-1}$ and the Rossby number is of order unity or greater. Therefore, it is not appropriate to assume that the Coriolis force balances the pressure gradient force. In fact, (11.5) through (11.8) show that if the pressure gradient force is to be balanced in (11.1), the geopotential perturbation must scale as $\delta + \Phi \sim U^2 \sim 100\,\mathrm{m}^2\,\mathrm{s}^{-2}$, and geopotential perturbations associated with equatorial synoptic-scale disturbances will be an order of magnitude smaller than those for midlatitude systems of similar scale.

This constraint on the amplitude of geopotential fluctuations in the tropics has profound consequences for the structure of synoptic-scale tropical motion systems. These consequences can be understood easily by applying scaling arguments to the thermodynamic energy equation. It is first necessary to obtain an estimate of the temperature fluctuations. The hydrostatic approximation (11.2) implies that for systems whose vertical scale is comparable to the scale height,

$$T = (H/R)\partial\Phi/\partial z^* \sim (\delta\Phi/R) \sim U^2/R \sim 0.3\,\mathrm{K} \tag{11.9}$$

Therefore, deep tropical systems are characterized by practically negligible synoptic-scale temperature fluctuations. Referring to the thermodynamic energy equation, we find that for such systems

$$\left(\frac{\partial}{\partial t} + \mathbf{V}\cdot\nabla\right) T \sim 0.3\,\mathrm{K\,d}^{-1}$$

In the absence of precipitation, the diabatic heating is caused primarily by the emission of long wave radiation, which tends to cool the troposphere at a rate of $J/c_p \sim 1\,\mathrm{K\,d}^{-1}$. Because the actual temperature fluctuations are small, this radiative cooling must be approximately balanced by adiabatic warming due to subsidence. Thus, to a first approximation, (11.4) becomes a diagnostic relationship for w^*:

$$w^*(N^2H/R) = J/c_p \tag{11.10}$$

For the tropical troposphere, $N^2H/R \sim 3\,\mathrm{K\,km}^{-1}$, so the vertical motion scale must satisfy $W \sim 0.3\,\mathrm{cm\,s}^{-1}$ and $WL/UH \sim 0.03$ in (11.6). Therefore, in the absence of precipitation, the vertical motion is constrained to be even smaller than in extratropical synoptic systems of a similar scale. Not only can the vertical advection term be neglected in (11.1), but from the continuity equation (11.3), the divergence of the horizontal wind is $\sim 3 \times 10^{-7}\,\mathrm{s}^{-1}$. Thus, the flow is nearly nondivergent.

The quasi-nondivergent nature of the flow in the absence of convective disturbances in the tropics makes it possible to simplify the governing equations

for that situation. A theorem of Helmholtz[3] states that any velocity field can be divided into a *nondivergent* part $\mathbf{V}_\psi$ and an i*rrotational* part $\mathbf{V}_e$ such that

$$\mathbf{V} = \mathbf{V}_\psi + \mathbf{V}_e$$

where $\nabla \cdot \mathbf{V}_\psi = 0$ and $\nabla \times \mathbf{V}_e = 0$.

For a two-dimensional velocity field the nondivergent part can be expressed in terms of a *streamfunction* ψ defined by letting

$$\mathbf{V}_\psi = \mathbf{k} \times \nabla\psi \tag{11.11}$$

or in Cartesian components:

$$u_\psi = -\partial\psi/\partial y, \quad v_\psi = \partial\psi/\partial x$$

from which it is verified easily that $\nabla \cdot \mathbf{V}_\psi = 0$ and $\zeta = \mathbf{k} \cdot \nabla \times \mathbf{V}_\psi = \nabla^2\psi$. Because the isolines of ψ correspond to streamlines for the nondivergent velocity and the distance separating the isolines of ψ is inversely proportional to the magnitude of the nondivergent velocity, the spatial distribution of $\mathbf{V}_\psi$ can be pictured easily by plotting lines of constant ψ on a synoptic chart.

We now approximate $\mathbf{V}$ by its nondivergent part $\mathbf{V}_\psi$ in (11.1) and neglect the small vertical advection term to obtain an approximate momentum equation valid for synoptic-scale motions in the tropics outside regions of precipitation:

$$\frac{\partial \mathbf{V}_\psi}{\partial t} + \left(\mathbf{V}_\psi \cdot \nabla\right)\mathbf{V}_\psi + f\mathbf{k} \times \mathbf{V}_\psi = -\nabla\Phi \tag{11.12}$$

Using the vector identity

$$(\mathbf{V} \cdot \nabla)\mathbf{V} = \nabla\left(\frac{\mathbf{V} \cdot \mathbf{V}}{2}\right) + \mathbf{k} \times \mathbf{V}\zeta$$

we can rewrite (11.12) as

$$\frac{\partial \mathbf{V}_\psi}{\partial t} = -\nabla\left(\Phi + \frac{\mathbf{V}_\psi \cdot \mathbf{V}_\psi}{2}\right) - \mathbf{k} \times \mathbf{V}_\psi\,(\zeta + f) \tag{11.13}$$

We next take $\mathbf{k} \cdot \nabla \times$ (11.13) to obtain the vorticity equation valid for nondivergent flow:

$$\left(\frac{\partial}{\partial t} + \mathbf{V}_\psi \cdot \nabla\right)(\zeta + f) = 0 \tag{11.14}$$

This equation shows that in the absence of condensation heating, synoptic-scale circulations in the tropics in which the vertical scale is comparable to the scale height of the atmosphere must be barotropic; absolute vorticity is conserved following the nondivergent horizontal wind. Such disturbances cannot convert

[3] See, for example, Bourne and Kendall (1968, p. 190).

potential energy to kinetic energy. They must be driven by barotropic conversion of mean-flow kinetic energy or by lateral coupling either to midlatitude systems or to precipitating tropical disturbances.

Because both the nondivergent velocity and the vorticity can be expressed in terms of the streamfunction, (11.14) requires only the field of ψ at any level in order to make a prediction. The pressure distribution is neither required nor predicted. Rather, it must be determined diagnostically. The relationship of the pressure and streamfunction fields can be obtained by taking $\nabla \cdot$ (11.13). This yields a diagnostic relationship between the geopotential and streamfunction fields, which is usually referred to as the *nonlinear balance equation*:

$$\nabla^2 \left[\Phi + \frac{1}{2} (\nabla \psi)^2 \right] = \nabla \cdot \left[\left(f + \nabla^2 \psi \right) \nabla \psi \right] \tag{11.15}$$

For the special case of stationary circularly symmetric flow, (11.15) is equivalent to the gradient wind approximation. Unlike the gradient wind, however, the balance in (11.15) does not require information on trajectory curvature and thus can be solved for Φ from knowledge of the instantaneous distribution of ψ on an isobaric surface. Alternatively, if the Φ distribution is known, (11.15) can be solved for ψ. In this case the equation is quadratic so that there are generally two possible solutions, which correspond to the normal and anomalous gradient wind cases.

Such a balance condition is valid only when the previous scaling arguments apply. These, however, have been based on the assumptions that the depth scale is comparable to the scale height of the atmosphere and that the horizontal scale is of order 1000 km. There is a special class of planetary-scale motions for which the divergence term in the vorticity equation is important even outside of regions of active precipitation (see Section 11.4). For such motions the pressure field cannot be diagnosed from a balance relationship. Rather, the pressure distribution must be predicted from the primitive equation form of the dynamics equations.

For precipitating synoptic-scale systems in the tropics, the preceding scaling considerations require extensive modification. Precipitation rates in such systems are typically of the order 2 cm d^{-1}. This implies condensation of $m_w = 20$ kg water for an atmospheric column of 1 m^2 cross-section. Because the latent heat of condensation is $L_c \approx 2.5 \times 10^6$ J kg^{-1}, this precipitation rate implies an addition of heat energy to the atmospheric column of

$$m_w L_c \sim 5 \times 10^7 \text{ J m}^{-2} \text{ d}^{-1}$$

If this heat is distributed uniformly over the entire atmospheric column of mass $p_0/g \approx 10^4$ kg m^{-2}, then the average heating rate per unit mass of air is

$$J/c_p \approx \left[L_c m_w / c_p \, (p_0/g) \right] \sim 5 \text{ K d}^{-1}$$

In reality the condensation heating due to deep convective clouds is not distributed evenly over the entire vertical column, but is a maximum between

300 and 400 hPa, where the heating rate can be as high as 10 K d^{-1}. In this case the approximate thermodynamic energy equation (11.10) implies that the vertical motion on the synoptic scale in precipitating systems must have a magnitude of order $W \sim 3\,\text{cm s}^{-1}$ in order that the adiabatic cooling can balance the condensation heating in the 300- to 400-hPa layer. Therefore, the average vertical motion in precipitating disturbances in the tropics is an order of magnitude larger than the vertical motion outside the disturbances. As a result the flow in these disturbances has a relatively large divergent component so that the barotropic vorticity equation (11.14) is no longer a reasonable approximation, and the full primitive equations must be used to analyze the flow.

11.3 CONDENSATION HEATING

The manner in which the atmosphere is heated by condensation of water vapor depends crucially on the nature of the condensation process. In particular, it is necessary to differentiate between latent heat release through large-scale vertical motion (i.e., synoptic-scale forced uplift) and the latent heat release due to deep cumulus convection. The former process, which is generally associated with midlatitude synoptic systems, can be incorporated easily into the thermodynamic energy equation in terms of the synoptic-scale field variables. The large-scale heating field resulting from the cooperative action of many cumulonimbus cells, however, requires representation of this type of latent heating in terms of the synoptic-scale field variables, which is much more difficult.

Before considering the problem of condensation heating by cumulus convection, it is worth indicating briefly how the condensation heating by large-scale forced uplift can be included in a prediction model. The approximate thermodynamic energy equation for a pseudoadiabatic process given in Section 2.9.1 states that

$$\frac{D \ln \theta}{Dt} \approx -\left(\frac{L_c}{c_p T}\right) \frac{Dq_s}{Dt} \tag{11.16}$$

It may be shown that an *equivalent static stability*, Γ_e, may be defined so that (11.16) can be written as

$$\left(\frac{\partial}{\partial t} + \mathbf{V} \cdot \nabla\right) \theta + w\Gamma_e \approx 0 \tag{11.17}$$

where

$$\Gamma_e \approx \begin{cases} (\Gamma_s / \Gamma_d)\, \partial\theta_e / \partial z & \text{for } q \geq q_s \text{ and } w > 0 \\ \partial\theta / \partial z & \text{for } q < q_s \text{ or } w < 0 \end{cases}$$

Here, Γ_s and Γ_d are the lapse rates for pseudoadiabatic and dry ascent, respectively. Thus, in the case of condensation due to large-scale forced ascent ($\Gamma_e > 0$), the thermodynamic energy equation has essentially the same form

as for adiabatic motions except that the static stability is replaced by the equivalent static stability. As a consequence, the local temperature changes induced by the forced ascent will be smaller than for the case of forced dry ascent with the same lapse rate.

If, however, $\Gamma_e < 0$, the atmosphere is conditionally unstable and condensation will occur primarily through cumulus convection. In that case, the vertical velocity must be that of the individual cumulus updrafts, not the synoptic-scale w. Thus, a simple formulation of the thermodynamic energy equation in terms of only the synoptic-scale variables is not possible. We can still, however, simplify the thermodynamic energy equation to some extent. We recall from Section 11.2—see Eq. (11.10)—that due to the smallness of temperature fluctuations in the tropics, the adiabatic cooling and diabatic heating terms must approximately balance. Thus, (11.16) becomes approximately

$$w\frac{\partial \ln\theta}{\partial z} \approx -\frac{L_c}{c_pT}\frac{Dq_s}{Dt} \tag{11.18}$$

The synoptic-scale vertical velocity w that appears in (11.18) is the average of very large vertical motions in the active convection cells and small vertical motions in the environment. Thus, if we let w' be the vertical velocity in the convective cells and the $\overline{w}$ be vertical velocity in the environment, we have

$$w = aw' + (1-a)\overline{w} \tag{11.19}$$

where a is the fractional area occupied by the convection. Approximating the change in q_s following the motion by $w\frac{\partial q_s}{\partial z}$, we can then write (11.18) in the form

$$w\frac{\partial \ln\theta}{\partial z} \approx -\frac{L_c}{c_pT}aw'\frac{\partial q_s}{\partial z} \tag{11.20}$$

The problem now is to express the condensation heating term on the right in (11.20) in terms of synoptic-scale field variables.

This problem of *parameterizing* the cumulus convective heating is one of the most challenging areas in tropical meteorology. A simple approach that has been used successfully in some theoretical studies[4] is based on the fact that, because the storage of water in the clouds is rather small, the total vertically integrated heating rate due to condensation must be approximately proportional to the net precipitation rate:

$$-\int_{z_c}^{z_T}\left(\rho aw'\partial q_s/\partial z\right)dz = P \tag{11.21}$$

where z_c and z_T represent the cloud base and cloud top heights, respectively, and P is the precipitation rate ($\mathrm{kg\,m^{-2}\,s^{-1}}$).

[4] See, for example, Stevens and Lindzen (1978).

Because relatively little moisture goes into changing the atmospheric vapor mixing ratio, the net precipitation rate must approximately equal the moisture convergence into an atmospheric column plus surface evaporation:

$$P = -\int_0^{z_m} \nabla \cdot (\rho q \mathbf{V}) dz + E \tag{11.22}$$

where E is the evaporation rate (kg m^{-2} s^{-1}) and z_m is the top of the moist layer ($z_m \approx 2$ km over much of the equatorial oceans). Substituting into (11.22) from the approximate continuity equation for q,

$$\nabla \cdot (\rho q \mathbf{V}) + \partial (\rho q w) / \partial z \approx 0 \tag{11.23}$$

we obtain

$$P = (\rho w q)_{z_m} + E \tag{11.24}$$

Using (11.24) we can relate the vertically averaged heating rate to the synoptic-scale variables $w(z_m)$ and $q(z_m)$.

We still, however, need to determine distribution of the heating in the vertical. The most common approach is to use an empirically determined vertical distribution based on observations. In that case, equation (11.16) can be written as

$$\left(\frac{\partial}{\partial t} + \mathbf{V} \cdot \nabla\right) \ln\theta + w \frac{\partial \ln\theta}{\partial z} = \frac{L_c}{\rho c_p T} \eta(z) \left[(\rho w q)_{z_m} + E\right] \tag{11.25}$$

where $\eta(z) = 0$ for $z < z_c$ and $z > z_T$ and $\eta(z)$ for $z_c \leq z \leq z_T$ is a weighting function that must satisfy

$$\int_{z_c}^{z_T} \eta(z) dz = 1$$

Recalling that the diabatic heating must be approximately balanced by adiabatic cooling as indicated in (11.20), we see from (11.25) that $\eta(z)$ will have a vertical structure similar to that of the large-scale vertical mass flux, ρw. Observations indicate that for many tropical synoptic-scale disturbances, $\eta(z)$ reaches its maximum at about the 400-hPa level, consistent with the divergence pattern shown earlier in Figure 11.5.

The preceding formulation is designed to model average tropical conditions. In reality, the vertical distribution of diabatic heating is determined by the local distribution of cloud heights. Thus, the cloud height distribution is apparently a key parameter in cumulus parameterization. A cumulus parameterization scheme in which this distribution is determined in terms of the large-scale variables was developed by Arakawa and Schubert (1974). A number of other schemes have been suggested in the past decade. Discussion of these is beyond the scope of this text.

11.4 EQUATORIAL WAVE THEORY

Equatorial waves are an important class of eastward- and westward-propagating disturbances in the atmosphere and in the ocean that are trapped about the equator (i.e., they decay away from the equatorial region). Diabatic heating by organized tropical convection can excite atmospheric equatorial waves, whereas wind stresses can excite oceanic equatorial waves. Atmospheric equatorial wave propagation can cause the effects of convective storms to be communicated over large longitudinal distances, thus producing remote responses to localized heat sources. Furthermore, by influencing the pattern of low-level moisture convergence, atmospheric equatorial waves can partly control the spatial and the temporal distribution of convective heating. Oceanic equatorial wave propagation, however, can cause local wind stress anomalies to remotely influence the thermocline depth and the sea surface temperature, as was discussed in Section 11.1.6.

11.4.1 Equatorial Rossby and Rossby–Gravity Modes

A complete development of equatorial wave theory would be rather complicated. In order to introduce equatorial waves in the simplest possible context, we here use a shallow water model, analogous to that introduced in Section 4.5, and concentrate on the *horizontal* structure. Vertical propagation in a stratified atmosphere is discussed in Chapter 12. For simplicity, we consider the linearized momentum and continuity equations for a fluid system of mean depth h_e in a motionless basic state. Because we are interested only in the tropics, we utilize Cartesian geometry on an *equatorial β plane* Section 5.7. In this approximation, terms proportional to cos ϕ are replaced by unity, and terms proportional to sin ϕ are replaced by y/a, where y is the distance from the equator and a is the radius of Earth. The Coriolis parameter in this approximation is given by

$$f \approx \beta y \tag{11.26}$$

where $\beta \equiv 2\Omega/a$, and Ω is the angular velocity of Earth. The resulting linearized shallow water equations (Section 4.5) for perturbations on a motionless basic state of mean depth h_e may be written as

$$\partial u'/\partial t - \beta y v' = -\partial \Phi'/\partial x \tag{11.27}$$

$$\partial v'/\partial t + \beta y u' = -\partial \Phi'/\partial y \tag{11.28}$$

$$\partial \Phi'/\partial t + g h_e \left(\partial u'/\partial x + \partial v'/\partial y\right) = 0 \tag{11.29}$$

where $\Phi' = gh'$ is the geopotential disturbance, and primed variables designate perturbation fields.

The x and t dependence may be separated by specifying solutions in the form of zonally propagating waves:

$$\begin{pmatrix} u' \\ v' \\ \Phi' \end{pmatrix} = \begin{bmatrix} \hat{u}(y) \\ \hat{v}(y) \\ \hat{\Phi}(y) \end{bmatrix} \exp[i(kx - \nu t)] \tag{11.30}$$

Substitution of (11.30) into (11.27), (11.28), and (11.29) then yields a set of ordinary differential equations in y for the meridional structure functions $\hat{u}$, $\hat{v}$, $\hat{\Phi}$:

$$-i\nu\hat{u} - \beta y\hat{v} = -ik\hat{\Phi} \tag{11.31}$$

$$-i\nu\hat{v} + \beta y\hat{u} = -\partial\hat{\Phi}/\partial y \tag{11.32}$$

$$-i\nu\hat{\Phi} + gh_e\left(ik\hat{u} + \partial\hat{v}/\partial y\right) = 0 \tag{11.33}$$

If (11.31) is solved for $\hat{u}$ and the result substituted into (11.32) and (11.33), we obtain

$$\left(\beta^2y^2 - \nu^2\right)\hat{v} = ik\beta y\hat{\Phi} + i\nu\partial\hat{\Phi}/\partial y \tag{11.34}$$

$$\left(\nu^2 - gh_ek^2\right)\hat{\Phi} + i\nu gh_e\left(\frac{\partial\hat{v}}{\partial y} - \frac{k}{\nu}\beta y\hat{v}\right) = 0 \tag{11.35}$$

Finally, (11.35) can be substituted into (11.34) to eliminate $\hat{\Phi}$, yielding a second-order differential equation in the single unknown, $\hat{v}$:

$$\frac{\partial^2\hat{v}}{\partial y^2} + \left[\left(\frac{\nu^2}{gh_e} - k^2 - \frac{k}{\nu}\beta\right) - \frac{\beta^2y^2}{gh_e}\right]\hat{v} = 0 \tag{11.36}$$

Because (11.36) is homogeneous, we expect that nontrivial solutions satisfying the requirement of decay at large $|y|$ will exist only for certain values of ν, corresponding to frequencies of the normal mode disturbances.

Before discussing this equation in detail, it is worth considering the asymptotic limits that occur when either $h_e \to \infty$ or $\beta = 0$. In the former case, which is equivalent to assuming that the motion is nondivergent, (11.36) reduces to

$$\frac{\partial^2\hat{v}}{\partial y^2} + \left[-k^2 - \frac{k}{\nu}\beta\right]\hat{v} = 0$$

Solutions exist of the form $\hat{v} \sim \exp(ily)$, provided that ν satisfies the Rossby wave dispersion relationship, $\nu = -\beta k/(k^2 + l^2)$. This illustrates that for nondivergent barotropic flow, equatorial dynamics is in no way special. Earth's rotation enters only in the form of the β effect; it is not dependent on f. However, if $\beta = 0$, all influence of rotation is eliminated and (11.36) reduces to the shallow water gravity wave model, which has nontrivial solutions for

$$\nu = \pm\left[gh_e\left(k^2 + l^2\right)\right]^{1/2}$$

Returning to (11.36), we seek solutions for the meridional distribution of $\hat{v}$, subject to the boundary condition that the disturbance fields vanish for $|y| \to \infty$. This boundary condition is necessary because the approximation $f \approx \beta y$ is not valid for latitudes much beyond $\pm 30^\circ$, so that solutions must be trapped equatorially if they are to be good approximations to the exact solutions on the sphere. Equation (11.36) differs from the classic equation for a harmonic oscillator in y because the coefficient in square brackets is not a constant but is a function of y. For sufficiently small y, this coefficient is positive and solutions oscillate in y, whereas for large y, solutions either grow or decay in y. Only the decaying solutions, however, can satisfy the boundary conditions.

It turns out[5] that solutions to (11.36), which satisfy the condition of decay far from the equator, exist only when the constant part of the coefficient in square brackets satisfies the relationship

$$\frac{\sqrt{gh_e}}{\beta}\left(-\frac{k}{\nu}\beta - k^2 + \frac{\nu^2}{gh_e}\right) = 2n+1; \quad n = 0,1,2,\ldots \tag{11.37}$$

which is a cubic dispersion equation determining the frequencies of permitted equatorially trapped free oscillations for zonal wave number k and meridional mode number n. These solutions can be expressed most conveniently if y is replaced by the nondimensional meridional coordinate

$$\xi \equiv \left(\beta \Big/ \sqrt{gh_e}\right)^{1/2} y$$

Then the solution has the form

$$\hat{v}(\xi) = v_0 \mathrm{H_n}(\xi) \exp\left(-\xi^2/2\right) \tag{11.38}$$

where v_0 is a constant with velocity units, and $\mathrm{H}_n(\xi)$ designates the nth *Hermite polynomial*. The first few of these polynomials have the values

$$\mathrm{H}_0 = 1, \quad \mathrm{H}_1(\xi) = 2\xi, \quad \mathrm{H}_2(\xi) = 4\xi^2 - 2$$

Thus, the index n corresponds to the number of nodes in the meridional velocity profile in the domain $|y| < \infty$.

In general the three solutions of (11.37) can be interpreted as eastward- and westward-moving equatorially trapped gravity waves, and westward-moving equatorial Rossby waves. The case $n = 0$ (for which the meridional velocity perturbation has a Gaussian distribution centered at the equator) must be treated separately. In this case the dispersion relationship (11.37) factors as

$$\left(\frac{\nu}{\sqrt{gh_e}} - \frac{\beta}{\nu} - k\right)\left(\frac{\nu}{\sqrt{gh_e}} + k\right) = 0 \tag{11.39}$$

[5] See Matsuno (1966).

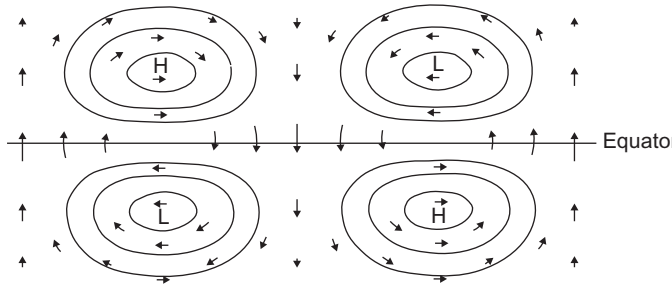

FIGURE 11.13 Plan view of horizontal velocity and height perturbations associated with an equatorial Rossby–gravity wave. (*Adapted from Matsuno, 1966. Used with permission of the Japan Society for the Promotion of Science.*)

The root $\nu/k = -\sqrt{gh_e}$, corresponding to a westward-propagating gravity wave, is not permitted, as the second term in parentheses in (11.39) was implicitly assumed not to vanish when (11.34) and (11.35) were combined to eliminate $\hat{\Phi}$. The roots given by the first term in parentheses in (11.39) are

$$\nu = k\sqrt{gh_e}\left[\frac{1}{2} \pm \frac{1}{2}\left(1 + \frac{4\beta}{k^2\sqrt{gh_e}}\right)^{1/2}\right] \tag{11.40}$$

The positive root corresponds to an eastward-propagating equatorial inertia–gravity wave, whereas the negative root corresponds to a westward-propagating wave, which resembles an inertia–gravity wave for long zonal scale ($k \to 0$) and resembles a Rossby wave for zonal scales characteristic of synoptic-scale disturbances. This mode is generally referred to as a *Rossby–gravity wave*. The horizontal structure of the westward-propagating $n = 0$ solution is shown in Figure 11.13, whereas the relationship between frequency and zonal wave number for this and several other equatorial wave modes is shown in Figure 11.14.

11.4.2 Equatorial Kelvin Waves

In addition to the modes discussed in the previous section, there is another equatorial wave that is of great practical importance. For this mode, which is called the equatorial *Kelvin wave*, the meridional velocity perturbation vanishes and (11.31), (11.32), and (11.33) are reduced to the simpler set

$$-i\nu\hat{u} = -ik\hat{\Phi} \tag{11.41}$$

$$\beta y\hat{u} = -\partial\hat{\Phi}/\partial y \tag{11.42}$$

$$-i\nu\hat{\Phi} + gh_e\left(ik\hat{u}\right) = 0 \tag{11.43}$$

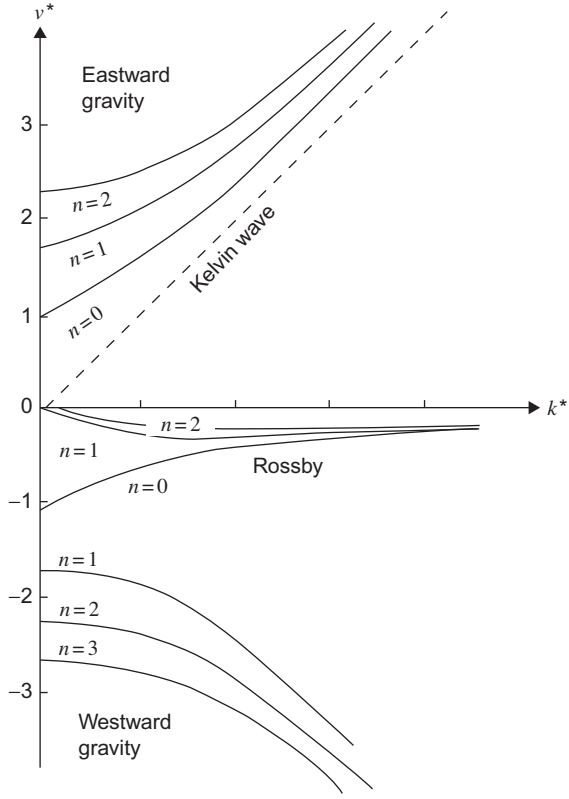

FIGURE 11.14 Dispersion diagram for free equatorial waves. Frequency and zonal wave numbers have been nondimensionalized by defining $\nu^* \equiv \nu/\left(\beta\sqrt{gh_e}\right)^{1/2}$ $k^* \equiv k\left(\sqrt{gh_e}/\beta\right)^{1/2}$. *Curves* show dependence of frequency on zonal wave number for eastward and westward gravity modes and for Rossby and Kelvin modes. (k^* axis tic marks at unit interval with 0 on left.)

Combining (11.41) and (11.43) to eliminate $\hat{\Phi}$, we see that the Kelvin wave dispersion equation is identical to that for ordinary shallow water gravity waves:

$$c^2 \equiv (\nu/k)^2 = gh_e \tag{11.44}$$

According to (11.44), the phase speed c can be either positive or negative. However, if (11.41) and (11.42) are combined to eliminate $\hat{\Phi}$, we obtain a first-order equation for determining the meridional structure:

$$\beta y\hat{u} = -c\partial\hat{u}/\partial y \tag{11.45}$$

which may be integrated immediately to yield

$$\hat{u} = u_o \exp\left(-\beta y^2/2c\right) \tag{11.46}$$

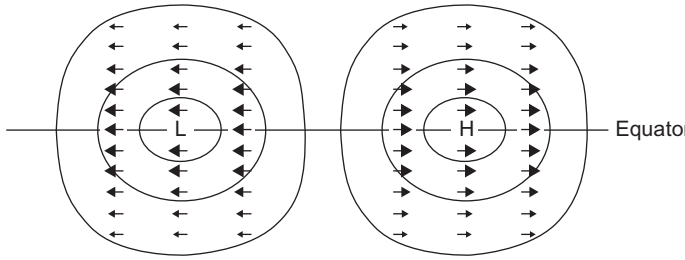

FIGURE 11.15 Plan view of horizontal velocity and height perturbations that are associated with an equatorial Kelvin wave. (*Adapted from Matsuno, 1966.*)

where u_0 is the amplitude of the perturbation zonal velocity at the equator. Equation (11.46) shows that if solutions decaying away from the equator are to exist, the phase speed must be positive ($c > 0$). Thus, Kelvin waves are eastward propagating and have zonal velocity and geopotential perturbations that vary in latitude as Gaussian functions centered on the equator. The e-folding decay width is given by

$$Y_K = |2c/\beta|^{1/2}$$

which for a phase speed $c = 30\,\mathrm{m\,s^{-1}}$ gives $Y_K \approx 1600$ km.

The perturbation wind and geopotential structure for the Kelvin wave are shown in plan view in Figure 11.15. In the zonal direction the force balance is exactly that of an eastward-propagating shallow water gravity wave. A vertical section along the equator would thus be the same as that shown in Figure 5.10. The meridional force balance for the Kelvin mode is an exact geostrophic balance between the zonal velocity and the meridional pressure gradient. It is the change in sign of the Coriolis parameter at the equator that permits this special type of equatorial mode to exist.

11.5 STEADY FORCED EQUATORIAL MOTIONS

Not all zonally asymmetric circulations in the tropics can be explained on the basis of inviscid equatorial wave theory. For quasi-steady circulations the zonal pressure gradient force must be balanced by turbulent drag rather than by inertia. The Walker circulation may be regarded as a quasi-steady equatorially trapped circulation that is generated by diabatic heating. The simplest models of such circulations specify the diabatic heating and use the equations of equatorial wave theory to compute the atmospheric response. These models, however, neglect the fact that the distribution of diabatic heating is highly dependent on the mean wind and equivalent potential temperature distributions in the boundary layer. These in turn depend on the surface pressure and the moisture distribution, which are themselves dependent on the motion field. Thus,

in a consistent model the diabatic heating cannot be regarded as an externally specified quantity, but must be obtained as part of the solution by, for example, using the cumulus parameterization scheme illustrated in Section 11.3.

As indicated in (11.25), this scheme requires information on the vertical distribution of convective heating in order to solve for the temperature perturbation throughout the troposphere. There is, however, evidence that the essential features of stationary equatorial circulations can be partly explained on the basis of a model that involves only the boundary layer. This is perhaps not surprising since the maintenance of a convective system depends on evaporation and moisture convergence in the boundary layer. Over the tropical oceans the boundary layer can be approximated as a mixed layer of about 2-km depth. This is capped by an inversion across which there is a density discontinuity $\delta\rho$ (see Figure 8.2). The virtual temperature in the mixed layer is strongly correlated with the sea surface temperature. If we assume that the pressure field is uniform at the top of the mixed layer, the surface pressure will be determined by hydrostatic mass adjustment within the mixed layer. The resulting pressure perturbation in the layer depends on the density discontinuity at the top of the layer and the deviation, h, of the layer depth from its mean depth H_b. In addition, there will be a contribution from the perturbation virtual potential temperature, θ_v, within the mixed layer. Thus, the perturbation geopotential in the mixed layer can be expressed as

$$\Phi = g\,(\delta\rho/\rho_0)\,h - \Gamma\theta_v \tag{11.47}$$

where $\Gamma \equiv (gH_b/\theta_0)$ is a constant and ρ_0 and θ_0 are constant mixed layer reference values of density and potential temperature, respectively.

According to (11.47), positive sea surface temperature anomalies and negative boundary layer height anomalies will produce low surface pressures and vice versa. If the boundary layer depth does not vary too much, the surface pressure gradient will thus tend to be proportional to the sea surface temperature gradient. The dynamics of steady circulations in such a mixed layer can be approximated by a set of linear equations analogous to the equatorial wave equations (11.27), (11.28), and (11.29), but with the time derivative terms replaced by linear damping terms.

Thus, in the momentum equations the surface eddy stress is taken to be proportional to the mean velocity in the mixed layer. In the continuity equation the perturbation in the mixed layer height is proportional to the mass convergence in the layer, with a coefficient that is smaller in the presence of convection than in its absence because of ventilation of the boundary layer by convection. The x and y components of the vertically averaged momentum equation for steady motions in the mixed layer can then be written as

$$\alpha u - \beta y v + \partial\Phi/\partial x = 0 \tag{11.48}$$

$$\alpha v + \beta y u + \partial\Phi/\partial y = 0 \tag{11.49}$$

whereas the continuity equation can be expressed as

$$\alpha h + H_b\,(1-\varepsilon)\,(\partial u/\partial x + \partial v/\partial y) = 0 \tag{11.50}$$

where ε is a coefficient that is zero in the absence of convection and of order 3/4 when convection occurs. Substituting from (11.47) into (11.50) yields

$$\alpha\Phi + c_b^2\,(1-\varepsilon)\,(\partial u/\partial x + \partial v/\partial y) = -\alpha\Gamma\theta_v \tag{11.51}$$

where $c_b^2 \equiv g\,(\delta\rho/\rho_0)\,H_b$ is the square of the phase speed for gravity waves propagating along the inversion at the top of the mixed layer. See Battisti et al. (1999) for a more complete discussion.

Equations (11.48), (11.49), and (11.51) are a closed set for prediction of the boundary layer variables u, v, Φ for a specified boundary layer perturbation virtual temperature θ_v. However, because the parameter ε depends on the presence or absence of convection, the system can only be solved by iteration through using (11.22) to test for the presence of convection. This model can be used to compute the steady surface circulation. A sample calculation of the anomalous circulation for temperature anomalies corresponding to a typical ENSO event is shown in Figure 11.16. Note that the region of convergence is narrower than the

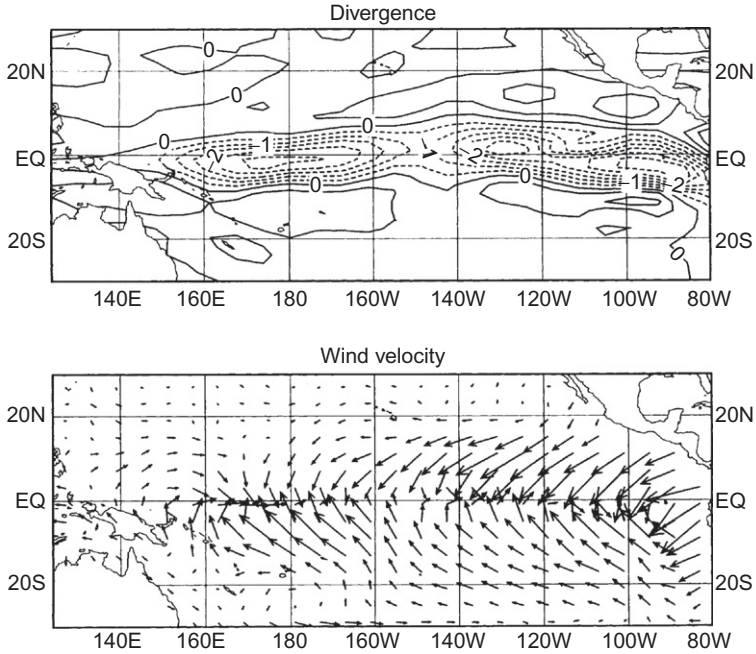

FIGURE 11.16 Steady surface circulation forced by sea surface temperature anomalies characteristic of El Niño in the equatorial Pacific. (*Courtesy of D. Battisti.*)

region of warm SST anomalies due to the convective feedback in the boundary layer model.

SUGGESTED REFERENCES

Philander, *El Niño, La Niña, and the Southern Oscillation*, is a well-written text that covers the dynamics of both atmospheric and oceanographic aspects of ENSO at an advanced level.

Trenberth (1991) is an excellent review article on ENSO.

Wallace (1971) is a detailed review of the structure of synoptic-scale tropospheric wave disturbances in the equatorial Pacific.

Webster and Fasullo (2003) present an excellent review of the structure and dynamics of tropical monsoons.

PROBLEMS

11.1. Suppose that the relative vorticity at the top of an Ekman layer at 15°N is $\zeta = 2 \times 10^{-5}\,\mathrm{s}^{-1}$. Let the eddy viscosity coefficient be $K_m = 10\,\mathrm{m}^2\,\mathrm{s}^{-1}$ and the water vapor mixing ratio at the top of the Ekman layer be $12\,\mathrm{g\,kg}^{-1}$. Use the method of Section 11.3 to estimate the precipitation rate due to moisture convergence in the Ekman layer.

11.2. As mentioned in Section 11.1.3, barotropic instability is a possible energy source for some equatorial disturbances. Consider the following profile for an easterly jet near the equator:

$$\bar{u}\,(y) = -u_0 \sin^2\left[l\,(y - y_0)\right]$$

where u_0, y_0, and l are constants and y is the distance from the equator. Determine the necessary conditions for this profile to be barotropically unstable.

11.3. Show that the nonlinear terms in the balance equation (11.15)

$$G\,(x, y) \equiv -\nabla^2\left(\frac{1}{2}\nabla\psi \cdot \nabla\psi\right) + \nabla \cdot \left(\nabla\psi\nabla^2\psi\right)$$

may be written in Cartesian coordinates as

$$G\,(x, y) = 2\left[\left(\partial^2\psi/\partial x^2\right)\left(\partial^2\psi/\partial y^2\right) - \left(\partial^2\psi/\partial x\partial y\right)^2\right]$$

11.4. With the aid of the results of Problem 11.3, show that if f is assumed to be constant the balance equation (11.15) is equivalent to the gradient wind equation (3.15) for a circularly symmetric regular low with geopotential perturbation given by

$$\Phi = \Phi_0\left(x^2 + y^2\right)\Big/L^2$$

where Φ_0 is a constant geopotential and L a constant length scale. *Hint:* Assume that $\psi(x, y)$ has the same functional dependence on (x, y) as does Φ.

11.5. Starting from the perturbation equations (11.27), (11.28), and (11.29), show that the sum of kinetic plus available potential energy is conserved for equatorial waves. Hence, show that for the Kelvin wave there is an equipartition of energy between kinetic and available potential energy.

11.6. Solve for the meridional dependence of the zonal wind and geopotential perturbations for a Rossby–gravity mode in terms of the meridional velocity distribution (11.38).

11.7. Use the linearized model (11.48) and (11.49) to compute the meridional distribution of divergence in the mixed layer for a situation in which the geostrophic wind is given by $u_g = u_o \exp\left(-\beta y^2/2c\right)$, $v_g = 0$, where u_0 and c are constants.

11.8. Show that the frequency of the $n = 1$ equatorial Rossby mode is given approximately by $\nu = -k\beta\left(k^2 + 3\beta/\sqrt{gh_e}\right)^{-1}$ and use this result to solve for the $\hat{u}(y)$ and $\hat{\Phi}(y)$ fields in terms of $\hat{v}(y)$. *Hint:* Use the fact that the Rossby wave phase speed is much less than $\sqrt{gh_e}$.

MATLAB Exercises

M11.1. The MATLAB script **profile_2.m** and the function **Tmoist.m** use December through March seasonal mean pressure and temperature data for Samoa (14°S, 171°W) in the file **tropical_temp.dat**, together with an assumed constant relative humidity of 80%, to calculate and graph vertical profiles of temperature, dewpoint, and the temperature corresponding to pseudoadiabatic ascent from the lifting condensation level for a parcel lifted from the lowest level of the sounding. Modify this script to plot profiles of the potential temperature, the equivalent potential temperature, and the saturation equivalent potential temperature. *Hint:* See Problem M9.2.

M11.2. For the thermodynamic sounding of Exercise M11.1, compute the CAPE and the profile of vertical velocity for a parcel lifted from the lowest layer in the absence of entrainment. What is the maximum vertical velocity and what is the distance that the parcel overshoots its level of neutral buoyancy? What can you conclude about convection associated with this mean tropical sounding?

M11.3. Consider a simple nondivergent flow given by the streamfunction $\psi = A \sin kx \sin ly$. The MATLAB script **nonlinear_balance.m** solves the nonlinear balance equation (11.15) for the corresponding geopotential Φ, assuming that the Coriolis parameter is a constant corresponding to its value at 30°N. Run this script for several values of the amplitude, A, in the range 0.4×10^7 to $4.0 \times 10^7\ \mathrm{m^2\,s^{-1}}$. Note how the geopotential field depends on A. For the case $A = 4.0 \times 10^7 \mathrm{m^2\,s^{-1}}$ use the **gradient** function in MATLAB to compute the geostrophic wind and thus find the ageostrophic wind. Plot these as quiver plots and explain why the ageostrophic wind has the structure seen in your plot.

M11.4. A simple model for the horizontal flow in the mixed layer on an equatorial β plane forced by an equatorial wave mode is given by the following equations:

$$\frac{\partial u}{\partial t} = -\alpha u + \beta y v - \frac{\partial \Phi}{\partial x}$$

$$\frac{\partial v}{\partial t} = -\alpha v - \beta y u - \frac{\partial \Phi}{\partial y}$$

where $\Phi(x, y, t)$ is given by (11.30) for the appropriate mode. The MATLAB script **equatorial_mixed_layer.m** solves these equations numerically for the horizontal velocity components and divergence field in the mixed layer forced by a specified Rossby–gravity wave ($n = 0$ mode) geopotential perturbation corresponding to a westward-propagating disturbance of zonal wavelength 4000 km and $\sqrt{gh_e} = 18\,\mathrm{m\,s^{-1}}$. Run the code for a long enough time so that the solution becomes periodic in time. Rerun the model for zonal wavelength 10,000 km and $\sqrt{gh_e} = 36\,\mathrm{m\,s^{-1}}$. In each case compare the frequency of the oscillation with the Coriolis parameter at the latitude of maximum convergence forced by the wave. What can you conclude from these results?

M11.5. Modify the MATLAB script of M11.4 to compute the mixed layer velocity and divergence pattern for the $n = 1$ Rossby mode for zonal wavelength 4000 km and $\sqrt{gh_e} = 18\,\mathrm{m\,s^{-1}}$ using the formulas for frequency and geopotential derived in Problem 11.8.

M11.6. The MATLAB script **forced_equatorial_mode2.m** shows the time development of the velocity and height perturbations produced by a transient localized mass source for shallow water waves on an equatorial β plane. The model is based on equations (11.48), (11.49), and (11.51), but with time tendency terms included ($\varepsilon = 0$ is set here, but you can experiment with different values if you wish). The source is located at the equator at $x = 0$. It rises smoothly in amplitude for the first 2.5 days and then decreases to 0 at day 5. Modify the script to contour the divergence and the vorticity. Run the script for a 10-day period and interpret the results in terms of equatorial wave theory by noting the structure and speeds of energy propagation for the disturbances to the east and west of the source.